Optimal Suppression Strategy for Capacitor Voltage Ripples of Hybrid MMCs Under Unbalanced Grid Voltages

Jianzhong Xu, *Senior Member*, *IEEE*, Junxin Wang, Yukun Yang, Jinan Wang, Gen Li*, *Member*, *IEEE*

***Abstract*—Submodule (SM) capacitor voltage ripples in modular multilevel converters (MMCs) can be suppressed by harmonic injection strategy, which can reduce the volume and cost of MMCs. The existing methods using the dual harmonic injection strategy for hybrid MMCs only consider steady-state conditions. Harmonic injection strategies for unbalanced grid voltage conditions only use single harmonic injection and can be applied for single-phase faults. To address the above issues, this paper proposes an optimal dual harmonic injection of second-order harmonic current and third-order harmonic voltage strategy for hybrid MMCs. Firstly, the mathematical model of MMC under unbalanced grid voltages is established. Then the ripple characteristics of SM capacitor voltage are analyzed to reveal the relationship between the capacitor voltage and the arm power ripples. Based on the developed instantaneous arm power model, optimal harmonic injection parameters are calculated. A hybrid MMC simulation model is built in PSCAD/EMTDC to verify the effectiveness of the proposed strategy. The results show the excellent performance of the proposed strategy in suppressing the voltage ripples under unbalanced voltage conditions.**

***Index Terms* — Hybrid MMC; capacitor voltage ripples; harmonic injection; unbalanced voltage conditions; instantaneous power of the arm.**

I. Introduction

MODULAR multi-level converters (MMCs) have become the preferred option for voltage-source-converter based high-voltage direct-current (VSC-HVDC) transmission systems [1], thanks to their merits of modularity, scalability, flexible control capability and low harmonics [2]-[4]. However, MMCs' weight, capital costs and power losses are still higher than their counterpart line commutated converter [5].

Submodule (SM) capacitors of MMCs account for more than 50% of the volume and about 40% of the cost [6], [7]. Suppressing the capacitor voltage ripples of SMs can reduce the capacitance and therefore, reduce the cost and volume/weight of MMCs. Thus, the research on the suppression strategy of MMC capacitor voltage fluctuation is of great significance [8], [9].

This work was supported by the Natural Science Foundation of Beijing Municipality (3220259) and the Central University Basic Research Fund of China (2020MS003). (*Corresponding author: Gen Li*)

J. Xu, J. Wang, Y. Yang and J. Wang are with the State Key Laboratory of Alternate Electrical Power System with Renewable Energy Sources, North China Electric Power University (NCEPU), Beijing, 102206, China. (e-mail: xujianzhong@ncepu.edu.cn).

G. Li is with the School of Engineering, Cardiff University, Cardiff, CF24 3AA. UK. (e-mail: Lig9@cardiff.ac.uk).

For half-bridge MMC (HB-MMC), due to the freewheeling diodes in HB-SMs, DC faults cannot be blocked like the full-bridge MMC (FB-MMC). However, FB-MMC requires more semiconductor devices and therefore, results in higher costs and power losses [10], [11]. The hybrid MMC consisting of HB-SMs and FB-SMs achieves a trade-off between the economy and technical performance [12], [13]. Hybrid MMC features in its flexible range of modulation index and DC fault handling capability [14], [15]. It has been deployed in the Kun-Liu-Long three-terminal ±800 kV ultra HVDC project in China [16]. The capital costs and weight of hybrid MMC can be further reduced if capacitor voltage ripples can be effectively suppressed.

New MMC topologies have been proposed to reduce the SM voltage ripples [17], [18]. However, the cost is still too high. Instead, control strategies for suppressing the ripples are cost-effective alternatives. For instance, the second-order harmonic current injection (SHCI), third-order harmonic voltage injection (THVI), and dual harmonic injection (DHI) of second-order harmonic current and third-order harmonic voltage [19]-[26].

For SHCI, by suppressing the unbalanced three-phase voltages, a circulating current suppressing controller has been proposed in [19], which can effectively suppress the capacitor voltage ripples. An SHCI is proposed in [20], wherein the injection reference is obtained by offline optimization to minimize the voltage ripples. Reference [21] proposes an online method to calculate the reference of SHCI, which avoids the use of a look-up table to determine the reference value. In [22], based on the mathematical model of hybrid MMC's capacitor voltage ripples, an optimized SHCI strategy is proposed.

The effect of THVI on regulating the capacitor voltage ripples has been analyzed in [23]. The study also shows that the MMC modulation index can be improved by injecting third-order harmonic voltage, which can reduce SM voltage ripples. However, the amplitude and phase of the injected third-order harmonic voltage are fixed and the adaptability to other operating conditions is not considered [24].

Reference [25] considers the DHI parameters determined in [20] and [24]. However, the coupling between the two parameter design methods is ignored. From the perspective of arm power, a DHI strategy is proposed in [26]. However, the method ignores the second-order harmonic voltage generated by arm inductors.

The above underpinning studies provide solid foundations for suppressing SM capacitor voltage ripples in hybrid MMCs. However, they only consider the control strategies for steady-state operation. The applicability of the strategies under unbalanced grid faults, which may lead to more severe SM voltage ripples, have not been analyzed.

Few research investigates the characteristics of SM voltage ripples of hybrid MMCs and DHI strategies under unbalanced grid voltages. Reference [27] analyzes the effect of MMC's circulating current on DC voltage oscillation under unbalanced grid voltages. In [28], the model of arm instantaneous power under grid-side single-line-to-ground (SLG) faults is developed and an SHCI method suitable for SLG faults is proposed. However, the work ignores the influence of the arm inductor voltage and THVI. [29] designs the MMC modulation index under SLG faults. However, this method will require a wide range of modulation index if it is applied in hybrid MMC because the negative voltage output capability of FB-SMs in hybrid MMC is limited. The studies in [20] and [21] only consider the single-phase voltage dip. Two-phase and three-phase voltage dips are not investigated. In addition, the studies in [28] show that the steady-state harmonic injection strategy may not be able to effectively suppress capacitor voltage ripples under unbalanced grid voltages, and even may aggravate the fluctuation of capacitor voltages. Therefore, capacitor voltage ripple suppression strategies for hybrid MMCs under unbalanced grid voltages considering the above issues should be proposed.

To bridge the above research gaps, this paper proposes an optimal DHI strategy to suppress capacitor voltage ripples under unbalanced grid voltages, which considers the second-order harmonic voltage generated on the arm inductor. By applying the strategy with optimized injection parameters, the instantaneous power fluctuations of three-phase arms can be suppressed, and the capacitor voltage ripples are reduced. Therefore, the SM capacitance can be greatly decreased. In addition, the overvoltage of the SMs under unbalanced voltage conditions is mitigated. The proposed methods are verified through simulations.

II. Basic Principles of MMC

A. Mathematical Model of MMC under Unbalanced Grid Voltages

A hybrid MMC is shown in Fig. 1. There are N SMs (p HB-SMs and q FB-SMs) in the upper and lower arms. u_i (i=a, b, c) is the AC side phase voltage, u_{pi} and u_{ni} are the upper and lower arm voltages, i_{pi} and i_{ni} are the upper and lower arm currents, U_{dc} is the DC voltage, I_{dc} is the DC current, L_{arm} is the arm inductor. The three-phase voltages on the grid-side can be expressed as:

$$\begin{cases} u_{ga} = x \cdot tU_m \sin(\omega t + \delta) \\ u_{gb} = y \cdot tU_m \sin(\omega t + \delta - 120^\circ) \\ u_{gc} = z \cdot tU_m \sin(\omega t + \delta + 120^\circ) \end{cases}, \quad (1)$$

where x, y and z are the three-phase voltage dip coefficients ranging from 0 to 1 and t is the transformer ratio. U_m is the amplitude of valve-side AC phase voltage under steady-state, ω is the fundamental angular frequency and δ is the shift angle due to the transformer wind configuration.

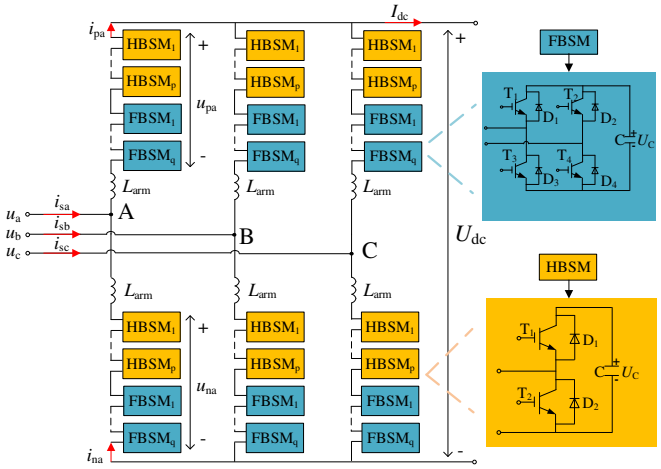

Fig. 1. Topology of the hybrid MMC.

Under steady-state conditions, the three-phase voltage dip coefficients are equal to 1. However, there will be negative-sequence voltages and currents under unbalanced grid voltages. The severity and modes of unbalanced voltages affect the dip coefficients and sequence components of the three-phase voltages.

The three-phase voltage can be decomposed by the symmetrical component method, which gives the positive, negative and zero sequence components of phase A:

$$\begin{bmatrix} u_{ga}^{+} \\ u_{ga}^{-} \\ u_{ga}^{0} \end{bmatrix} = \frac{1}{3} \begin{bmatrix} 1 & \alpha & \alpha^2 \\ 1 & \alpha^2 & \alpha \\ 1 & 1 & 1 \end{bmatrix} \begin{bmatrix} u_{ga} \\ u_{gb} \\ u_{gc} \end{bmatrix}, \quad (2)$$

where u_{ga}^{+}, u_{ga}^{-} and u_{ga}^{0} are the positive, negative and zero sequence voltage components of the grid-side phase A and $\alpha = e^{j120^\circ}$.

Due to the use of the Star-Delta (Y-Δ) transformer, there is no zero-sequence voltage on the converter valve-side, namely u_{ga}^{0} is zero. Considering that there is a shift angle δ on the primary and secondary sides of the transformer, the three-phase AC voltage on the valve side can be calculated as follows:

$$\begin{cases} u_a = U_{am}^{+} \sin(\omega t + \alpha^{+}) + U_{am}^{-} \sin(\omega t + \alpha^{-}) \\ u_b = U_{bm}^{+} \sin(\omega t + \beta^{+}) + U_{bm}^{-} \sin(\omega t + \beta^{-}) \\ u_c = U_{cm}^{+} \sin(\omega t + \gamma^{+}) + U_{cm}^{-} \sin(\omega t + \gamma^{-}) \end{cases}, \quad (3)$$

where U_{im}^{+} and U_{im}^{-} (i=a, b, c) are the amplitudes of three-phase positive and negative sequence voltage on the valve side. α^{+} & α^{-}, β^{+} & β^{-} and γ^{+} & γ^{-} are the phase angles of the positive and negative sequence voltages in phases A, B, C.

B. Analysis of Unbalanced Voltage Conditions

The general expression of MMC valve-side AC voltages is provided in (3). This subsection takes the SLG fault as an example for analysis, and the calculation process for other operating conditions can be analyzed similarly.

The shift angle δ of the Y-Δ connected transformer is 30°. If a solid SLG fault occurs in phase A, its voltage will drop to 0 and B-phase and C-phase voltages remain unchanged, that is,

x=0, y=z=1, so the three-phase voltages on the grid-side can be expressed as:

$$\begin{cases} u_{\mathrm{ga}} = 0 \\ u_{\mathrm{gb}} = tU_{\mathrm{m}} \sin(\omega t + 30^{\circ} - 120^{\circ}) \\ u_{\mathrm{gc}} = tU_{\mathrm{m}} \sin(\omega t + 30^{\circ} + 120^{\circ}) \end{cases}. \tag{4}$$

Using equation (2) to decompose the voltage sequence components, the positive, negative and zero-sequence components of phase A on the grid-side can be obtained as follows:

$$\begin{cases} u_{\mathrm{ga}}^{+} = \dfrac{2}{3} tU_{\mathrm{m}} \sin(\omega t + 30^{\circ}) \\ u_{\mathrm{ga}}^{-} = -\dfrac{1}{3} tU_{\mathrm{m}} \sin(\omega t + 30^{\circ}) \\ u_{\mathrm{ga}}^{0} = -\dfrac{1}{3} tU_{\mathrm{m}} \sin(\omega t + 30^{\circ}) \end{cases}. \tag{5}$$

The positive and negative sequence components of the other two phase voltages can be calculated using the rotation factor α. The three-phase AC voltages on the valve-side can be expressed as:

$$\begin{cases} u_{\mathrm{a}} = \dfrac{2}{3} U_{\mathrm{m}} \sin \omega t + \dfrac{1}{3} U_{\mathrm{m}} \sin(\omega t - 120^{\circ}) \\ u_{\mathrm{b}} = \dfrac{2}{3} U_{\mathrm{m}} \sin(\omega t - 120^{\circ}) + \dfrac{1}{3} U_{\mathrm{m}} \sin \omega t \\ u_{\mathrm{c}} = \dfrac{2}{3} U_{\mathrm{m}} \sin(\omega t + 120^{\circ}) + \dfrac{1}{3} U_{\mathrm{m}} \sin(\omega t + 120^{\circ}) \end{cases}. \tag{6}$$

The above analysis is based on the SLG fault in phase A. If two- or three-phase voltage dips occur in the grid side, the analysis is similar to the SLG fault in phase A. The three-phase voltages on the valve-side of two- or three-phase voltage dips conditions can be obtained by rewriting the grid-side voltages of (4), and then using (2) to decompose the voltage sequence components.

III. Analysis of SMs Capacitor Voltage Ripples

The arm power fluctuation is positively correlated with the amplitude of capacitor voltage ripples. The second-order harmonic voltage on the arm inductor will affect the arm power. However, the existing harmonic injection algorithm mainly considers the fundamental-frequency and the double-frequency fluctuations of the arm power. Ignoring the inductor voltage will affect the effect of the harmonic injection strategy, and cannot fully use its advantages. In addition, for using DHI, when the amplitude of the THVI is small, the deviation caused by ignoring the inductor voltage will be more obvious. Therefore, this section will firstly establish the arm power model considering the DHI and second-order harmonic voltage.

A. Arm Power Model Considering Dual Harmonic Injection and Second-order Harmonic Voltage

The DHI strategy refers to the injection of a second-order harmonic current into the arm and a third-order harmonic voltage into the AC voltage. The injection will reshape the waveforms of arm currents and voltages. According to the hybrid MMC topology illustrated in Fig. l, with the direction labelled in the diagram as the positive direction and considering the injection of the second-order harmonic current, the upper and lower arm currents i_{pa} and i_{na} in phase A can be expressed as:

$$\begin{cases} i_{\mathrm{pa}} = I_{\mathrm{dca}} + \dfrac{I_{\mathrm{m}}}{2} \sin(\omega t - \varphi) + I_2 \sin(2\omega t + \varphi_2) \\ i_{\mathrm{na}} = I_{\mathrm{dca}} - \dfrac{I_{\mathrm{m}}}{2} \sin(\omega t - \varphi) + I_2 \sin(2\omega t + \varphi_2) \end{cases}, \tag{7}$$

where i_{pa} and i_{na} are the upper and lower arm currents of phase A, φ and φ_2 are the power factor angle and the second-order harmonic current phase angle, I_{dca} is the DC current component of phase A, I_{m} is the amplitude of AC current under steady state and I_2 is the amplitude of the second-order harmonic current.

The modulation index m is defined as $2U_{\mathrm{m}}/U_{\mathrm{dc}}$, and the relationship between the AC and DC currents under steady-state conditions can be obtained as follows:

$$I_{\mathrm{dc}} = \frac{3}{4} m \cos\varphi I_{\mathrm{m}}. \tag{8}$$

According to equation (3), taking into account the THVI and the second-order harmonic voltage generated by the circulating current on the arm inductor, the upper and lower arm voltages u_{pa} and u_{na} can be expressed as:

$$\begin{cases} u_{\mathrm{pa}} = \dfrac{1}{2} U_{\mathrm{dc}} - U_{\mathrm{am}}^{+} \sin(\omega t + \alpha^{+}) - U_{\mathrm{am}}^{-} \sin(\omega t + \alpha^{-}) \\ -U_3 \sin(3\omega t + \varphi_3) + L_{\mathrm{arm}} \dfrac{di_{\mathrm{cir}}}{dt} \\ u_{\mathrm{na}} = \dfrac{1}{2} U_{\mathrm{dc}} + U_{\mathrm{am}}^{+} \sin(\omega t + \alpha^{+}) + U_{\mathrm{am}}^{-} \sin(\omega t + \alpha^{-}) \\ +U_3 \sin(3\omega t + \varphi_3) + L_{\mathrm{arm}} \dfrac{di_{\mathrm{cir}}}{dt} \end{cases}, \tag{9}$$

where U_3 is the amplitude of the third-order harmonic voltage, φ_3 is the phase angle of third-order harmonic voltage and i_{cir} is the injection of second-order harmonic current. It should be mentioned that as the amplitude of the fundamental-frequency component of the inductor voltage is much smaller than the AC voltage the voltage drop across the inductance caused by the fundamental-frequency current is ignored in (9).

In order to simplify the expression, making the following definitions:

$$\begin{cases} k_2 = \dfrac{2I_2}{I_{\mathrm{m}}} \\ k_3 = \dfrac{2U_3}{U_{\mathrm{dc}}} \\ c = \dfrac{8\omega L_{\mathrm{arm}} P_{\mathrm{dc}}}{3m\cos\varphi U_{\mathrm{dc}}^2} \end{cases}, \tag{10}$$

where k_2 and k_3 are the SHCI and THVI coefficients respectively. c is a constant, determined by the DC power P_{dc} and the DC voltage U_{dc}.

Taking the upper arm of phase A as an example, the arm voltage and current can be simplified as follows:

$$\begin{cases} i_{\mathrm{pa}} = \dfrac{I_{\mathrm{m}}}{2}[I_{\mathrm{dc\_a}} + \sin(\omega t - \varphi) + k_2 \sin(2\omega t + \varphi_2)] \\ u_{\mathrm{pa}} = \dfrac{U_{\mathrm{dc}}}{2}[1 - m_{\mathrm{a}}^{+} \sin(\omega t + \alpha^{+}) - m_{\mathrm{a}}^{-} \sin(\omega t + \alpha^{-}) \\ -k_3 \sin(3\omega t + \varphi_3) + ck_2 \cos(2\omega t + \varphi_2)] \end{cases}, \tag{11}$$

where $I_{\mathrm{dc\_a}}$ is the DC component of the *A*-phase arm current, m_a^+ and m_a^- are the positive and negative sequence voltage modulation index of phase *A*.

According to the expression of the arm current and voltage in equation (11), the instantaneous power P_{pa} of the upper arm in phase *A* can be obtained:

$$P_{\mathrm{pa}} = \frac{U_{\mathrm{dc}} I_{\mathrm{m}}}{4} \sum_{i=0}^{5} k_{\mathrm{pa}\_i} . \tag{12}$$

The specific expressions for each component of the above equation are given below:

$$\begin{cases} k_{\mathrm{pa\_0}} = I_{\mathrm{dc\_a}} - \dfrac{m_{\mathrm{a}}^{+} \cos(\alpha^{+} + \varphi) + m_{\mathrm{a}}^{-} \cos(\alpha^{-} + \varphi)}{2} \\ k_{\mathrm{pa\_1}} = \sin(\omega t - \varphi) - I_{\mathrm{dc\_a}} m_{\mathrm{a}}^{+} \sin(\omega t + \alpha^{+}) \\ -\dfrac{m_{\mathrm{a}}^{+} k_2}{2} \cos(\omega t + \varphi_2 - \alpha^{+}) - I_{\mathrm{dc\_a}} m_{\mathrm{a}}^{-} \sin(\omega t + \alpha^{-}) \\ -\dfrac{m_{\mathrm{a}}^{-} k_2}{2} \cos(\omega t + \varphi_2 - \alpha^{-}) - \dfrac{k_2 k_3}{2} \cos(\omega t + \varphi_3 - \varphi_2) \\ -\dfrac{ck_2}{2} \sin(\omega t + \varphi + \varphi_2) \\ k_{\mathrm{pa\_2}} = k_2 \sin(2\omega t + \varphi_2) + \dfrac{m_{\mathrm{a}}^{+}}{2} \cos(2\omega t + \alpha^{+} - \varphi) \\ +\dfrac{m_{\mathrm{a}}^{-}}{2} \cos(2\omega t + \alpha^{-} - \varphi) - \dfrac{k_3}{2} \cos(2\omega t + \varphi_3 + \varphi) \\ +I_{\mathrm{dc\_a}} ck_2 \cos(2\omega t + \varphi_2) \\ k_{\mathrm{pa\_3}} = \dfrac{m_{\mathrm{a}}^{+} k_2}{2} \cos(3\omega t + \varphi_2 + \alpha^{+}) - I_{\mathrm{dc\_a}} k_3 \sin(3\omega t + \varphi_3) \\ +\dfrac{m_{\mathrm{a}}^{-} k_2}{2} \cos(3\omega t + \varphi_2 + \alpha^{-}) + \dfrac{ck_2}{2} \sin(3\omega t + \varphi_2 - \varphi) \\ k_{\mathrm{pa\_4}} = \dfrac{k_3}{2} \cos(4\omega t + \varphi_3 - \varphi) + \dfrac{ck_2^2}{2} \sin(4\omega t + 2\varphi_2) \\ k_{\mathrm{pa\_5}} = \dfrac{k_2 k_3}{2} \cos(5\omega t + \varphi_2 + \varphi_3) \end{cases} . \tag{13}$$

Since the energy on the SMs cannot accumulate infinitely, the DC component should be zero. The DC component in the arm of phase *A* can be obtained as:

$$I_{\mathrm{dc\_a}} = \frac{m_{\mathrm{a}}^{+} \cos(\alpha_{\mathrm{a}}^{+} + \varphi) + m_{\mathrm{a}}^{-} \cos(\alpha_{\mathrm{a}}^{-} + \varphi)}{2} . \tag{14}$$

The above expressions are all based on phase *A*. If the values of three-phase voltage dips are not the same, the instantaneous arm power of the three phases will also be unbalanced. However, the calculation process of other two phases is similar. The expressions of phases *B* and *C* can be obtained by modifying the modulation index and phase angle of the positive and negative sequence voltages in equations (11)-(13).

B. Relationship Between the Arm Instantaneous Power and Capacitor Voltage Ripples

Due to the symmetry of the upper and lower arms of the MMC, it is reasonable to analyze the energy fluctuations only in the upper arm [26]. The relationship between the instantaneous power and the capacitor voltage ripples of the upper arm of phase *A* is as follows:

$$\frac{N}{2} C_0 (U_0 + \varepsilon)^2 - \frac{N}{2} C_0 (U_0 - \varepsilon)^2 = \int P_{\mathrm{pa}} dt , \tag{15}$$

where U_0 is the average value of the SM capacitor voltage, C_0 is the SM capacitance, N is the number of SMs in the arm and ε is the amplitude of capacitor voltage fluctuation. The SM capacitor voltage ripples can be changed by varying the arm instantaneous power which is obtained by multiplying u_{pa} and i_{pa}. Therefore, the SM capacitor voltage ripples can be changed by varying the arm voltages and currents. The capacitance C_0 can be solved by (15) [26]:

$$C_0 = \frac{P_s}{3mN\omega\eta(U_{\mathrm{c}})^2} [1 - (\frac{m\cos\varphi}{2})^2]^{\frac{3}{2}} , \tag{16}$$

where P_s is the apparent power of the converter, η is the percentage of capacitor voltage fluctuation and U_{c} is the SM capacitor voltage.

As can be seen from equation (16), the SM capacitance is closely related to capacitor voltage ripples. The smaller the capacitor voltage ripples, the smaller the SM capacitance is needed.

C. Influence of the Second-order Harmonic Voltage

To illustrate the influence of the second-order harmonic voltage, this subsection takes the steady-state condition as an example. The waveforms of the harmonic voltage and arm power are shown in Fig. 2. (Note: The simulations are carried out based on the parameters in Section V.A. The parameters of (k_2, k_3, φ_2, φ_3, m) are (0.6, 0.1, -90°, 0, 0.85) and the power factor cosφ is 1). The harmonic voltage and arm power are in per unit with the base of $U_{\mathrm{dc}}/2$ and P_{s}.

According to Fig. 2, the amplitude of the second-order harmonic voltage under these injection parameters is larger than the third-order harmonic voltage. In this case, ignoring the second-order harmonic voltage will lead to a large deviation between the theoretical and actual arm power. However, considering the second-order harmonic voltage can effectively compensate for the deviation. It also indicates that the second harmonic voltage cannot be ignored when the SHCI parameter is not small.

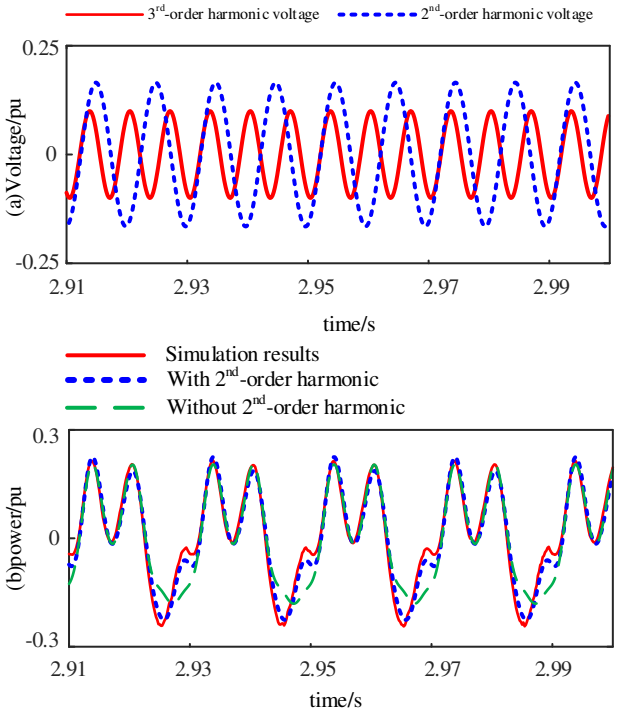

Fig. 2. Waveforms of harmonic voltage and arm power. (a) Harmonic voltage, (b) arm power.

IV. Optimal SM Capacitor Voltage Ripples Suppression Strategy with DHI

As can be seen from the analysis in Section III, the harmonic components of the arm instantaneous power are related to the capacitor voltage ripples. As shown in (13), due to the injection of dual harmonics, the third-order harmonic component of the arm power is generated. Therefore, to effectively suppress the power fluctuations of the arm, not only the fundamental-frequency and the double-frequency components will be considered, but also the triple-frequency component. In this section, the DHI parameter optimization process is analyzed based on the arm instantaneous power.

A. Extraction of Arm Instantaneous Power Fluctuations

In (13), the fundamental-frequency, double-frequency and triple-frequency components $P_{\text{pa\_1}}$, $P_{\text{pa\_2}}$ and $P_{\text{pa\_3}}$ of instantaneous power can be obtained. According to the orthogonal transformation, $P_{\text{pa\_1}}$, $P_{\text{pa\_2}}$ and $P_{\text{pa\_3}}$ can be rewritten as follows:

$$P_{\text{pa\_1}} = A_{\text{pa\_1}} \sin \omega t + B_{\text{pa\_1}} \cos \omega t$$

$$\begin{cases} A_{\text{pa\_1}} = \cos\varphi - I_{\text{dc\_a}} m_{\text{a}}^{+} \cos\alpha^{+} - I_{\text{dc\_a}} m_{\text{a}}^{-} \cos\alpha^{-} \\ + \dfrac{m_{\text{a}}^{+} k_2 \sin(\varphi_2 - \alpha^{+})}{2} + \dfrac{m_{\text{a}}^{-} k_2 \sin(\varphi_2 - \alpha^{-})}{2} \\ + \dfrac{k_2 k_3 \sin(\varphi_3 - \varphi_2)}{2} - \dfrac{c k_2 \cos(\varphi + \varphi_2)}{2} \\ B_{\text{pa\_1}} = -\sin\varphi - I_{\text{dc\_a}} m_{\text{a}}^{+} \sin\alpha^{+} - I_{\text{dc\_a}} m_{\text{a}}^{-} \sin\alpha^{-} \\ - \dfrac{m_{\text{a}}^{+} k_2 \cos(\varphi_2 - \alpha^{+})}{2} - \dfrac{m_{\text{a}}^{-} k_2 \cos(\varphi_2 - \alpha^{-})}{2} \\ - \dfrac{k_2 k_3 \cos(\varphi_3 - \varphi_2)}{2} - \dfrac{c k_2 \sin(\varphi + \varphi_2)}{2} \end{cases}, \quad (17)$$

$$P_{\text{pa\_2}} = A_{\text{pa\_2}} \sin 2\omega t + B_{\text{pa\_2}} \cos 2\omega t$$

$$\begin{cases} A_{\text{pa\_2}} = k_2 \cos\varphi_2 - \dfrac{m_{\text{a}}^{+} \sin(\alpha^{+} - \varphi)}{2} \\ - \dfrac{m_{\text{a}}^{-} \sin(\alpha^{-} - \varphi)}{2} + \dfrac{k_3 \sin(\varphi_3 + \varphi)}{2} - I_{\text{dc\_a}} c k_2 \sin\varphi_2 \\ B_{\text{pa\_2}} = k_2 \sin\varphi_2 + \dfrac{m_{\text{a}}^{+} \cos(\alpha^{+} - \varphi)}{2} \\ + \dfrac{m_{\text{a}}^{-} \cos(\alpha^{-} - \varphi)}{2} - \dfrac{k_3 \cos(\varphi_3 + \varphi)}{2} + I_{\text{dc\_a}} c k_2 \sin\varphi_2 \end{cases}, \quad (18)$$

$$P_{\text{pa\_3}} = A_{\text{pa\_3}} \sin 3\omega t + B_{\text{pa\_3}} \cos 3\omega t$$

$$\begin{cases} A_{\text{pa\_3}} = -\dfrac{k_2 m_{\text{a}}^{+} \sin(\alpha^{+} + \varphi_2)}{2} - I_{\text{dc\_a}} k_3 \cos\varphi_3 \\ - \dfrac{k_2 m_{\text{a}}^{-} \sin(\alpha^{-} + \varphi_2)}{2} + \dfrac{c k_2 \cos(\varphi_2 - \varphi)}{2} \\ B_{\text{pa\_3}} = \dfrac{k_2 m_{\text{a}}^{+} \cos(\alpha^{+} + \varphi_2)}{2} - I_{\text{dc\_a}} k_3 \sin\varphi_3 \\ + \dfrac{k_2 m_{\text{a}}^{-} \cos(\alpha^{-} + \varphi_2)}{2} + \dfrac{c k_2 \sin(\varphi_2 - \varphi)}{2} \end{cases} \quad (19)$$

Based on (17)-(19), the amplitudes of the fundamental-frequency, double-frequency and triple-frequency fluctuations of the arm instantaneous power of phase *A* can be obtained as follows:

$$\begin{cases} \left|P_{\text{pa\_1}}\right| = \sqrt{A_{\text{pa\_1}}^{\ 2} + B_{\text{pa\_1}}^{\ 2}} \\ \left|P_{\text{pa\_2}}\right| = \sqrt{A_{\text{pa\_2}}^{\ 2} + B_{\text{pa\_2}}^{\ 2}} \\ \left|P_{\text{pa\_3}}\right| = \sqrt{A_{\text{pa\_3}}^{\ 2} + B_{\text{pa\_3}}^{\ 2}} \end{cases}. \quad (20)$$

Similarly, the fundamental-frequency, double-frequency and triple-frequency components of the instantaneous power of phases *B* and *C* can be obtained similarly. Finally, the amplitudes $P_{\text{pb\_1}}$, $P_{\text{pb\_2}}$, $P_{\text{pb\_3}}$ and $P_{\text{pc\_1}}$, $P_{\text{pc\_2}}$, $P_{\text{pc\_3}}$ can be expressed as:

$$\begin{cases} \left|P_{\text{pb\_1}}\right| = \sqrt{A_{\text{pb\_1}}^{\ 2} + B_{\text{pb\_1}}^{\ 2}} \\ \left|P_{\text{pb\_2}}\right| = \sqrt{A_{\text{pb\_2}}^{\ 2} + B_{\text{pb\_2}}^{\ 2}} \\ \left|P_{\text{pb\_3}}\right| = \sqrt{A_{\text{pb\_3}}^{\ 2} + B_{\text{pb\_3}}^{\ 2}} \end{cases}, \quad (21)$$

$$\begin{cases} \left|P_{\text{pc\_1}}\right| = \sqrt{A_{\text{pc\_1}}^{\ 2} + B_{\text{pc\_1}}^{\ 2}} \\ \left|P_{\text{pc\_2}}\right| = \sqrt{A_{\text{pc\_2}}^{\ 2} + B_{\text{pc\_2}}^{\ 2}} \\ \left|P_{\text{pc\_3}}\right| = \sqrt{A_{\text{pc\_3}}^{\ 2} + B_{\text{pc\_3}}^{\ 2}} \end{cases}. \quad (22)$$

B. Optimal DHI

If the grid voltages are unbalanced, the instantaneous power of the three-phase arm will no longer be symmetrical. Therefore, it is necessary to consider the three-phase arm power at the same time. To minimize the amplitude of the three-phase power fluctuations, the objective function can be defined as:

$$P(k_2, \varphi_2, k_3, \varphi_3, m) = \sum \left|P_{\text{px\_1}}\right| + \sum \left|P_{\text{px\_2}}\right| + \sum \left|P_{\text{px\_3}}\right|, \quad (23)$$

where $|P_{px\_1}|$, $|P_{px\_2}|$ and $|P_{px\_3}|$ are the amplitudes of the fundamental, double and triple-frequency fluctuations of the three-phase upper arm, where x=a, b, c.

The minimization of equation (23) is used as the objective to obtain the optimal amplitude and phase of the DHI. The optimal values of m, k_2, φ_2, k_3 and φ_3 are determined according to different positive-sequence and negative-sequence modulation indexes and power factors. In this paper, the method of traversal parameters is taken as an example to explain how to determine the injection parameters in detail.

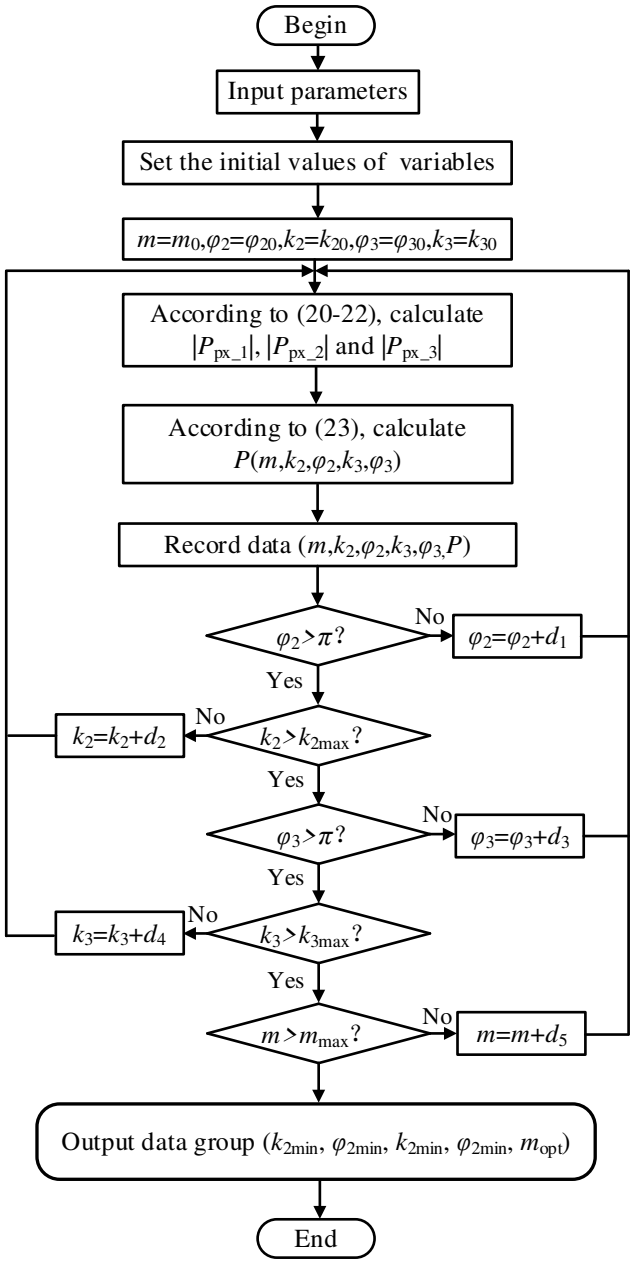

Fig. 3. Flow chart of the optimal process.

The optimization process of injection parameters is shown in Fig. 3. Firstly, system parameters will be input, including the positive-sequence and negative-sequence modulation index and phase angles of the three-phase voltages and the power factor, and the initial values of the variables and the traversal steps are determined. Set $\varphi_2 \in [-\pi, \pi]$, $k_2 \in [-1,1]$, $\varphi_3 \in [-\pi, \pi]$, $k_3 \in [-0.5,0.5]$, $m \in [1, 1.5]$, φ_{20}, k_{20}, φ_{30}, k_{30} and m_0 are the initial values of φ_2, k_2, φ_3, k_3 and m (φ_{20}=0, k_{20}=-1, φ_{30}=0, k_{30}=-0.5, m_0=1). d_1, d_2, d_3, d_4 and d_5 are the traversal steps of corresponding variables. The variables are then substituted into (20)-(22) to calculate the amplitudes of the fluctuations of the three-phase arm power. The value of the objective function P is calculated by substituting $|P_{px\_1}|$, $|P_{px\_2}|$ and $|P_{px\_3}|$ into equation (23), and the values are recorded as a data group (k_2, φ_2, k_3, φ_3, m, P) with the corresponding variables. Then the values of k_2, φ_2, k_3, φ_3 and m are updated and the above process is repeated to obtain the optimal injection parameters (k_{2min}, φ_{2min}, k_{2min}, φ_{2min}) and the optimal modulation index m_{opt} by finding the data group that makes the minimum value of the objective function P.

Fig. 4 shows the control diagram of DHI within the control system of the hybrid MMC. Using the DHI parameter optimization in Fig. 3, the optimal amplitude k_2 and phase φ_2 of the SHCI can be obtained. Then, reference signals i_{2fd_ref} and i_{2fq_ref} can be generated by the reference signal generator, where i_{2fd_ref} is the reference of the d-axis SHCI controller. i_{2fq_ref} is the reference signal of the q-axis SHCI controller. The reference is injected into the controller to obtain the voltage signal U_{cirj_ref}. Using the obtained optimal k_3 and φ_3, the THVI modulation signal U_{3j_ref} is obtained by THVI controller. Finally, the DHI is accomplished by altering the modulation wave of the modulation algorithm.

It should be noted that if the optimized modulation index m_{opt} > 1, the arm voltages of three phases may need to generate the negative voltages. At this time, only FBSMs participate in the process of modulation, and all HBSMs are bypassed [30], thus resulting in difference between the capacitor voltages of FBSMs and HBSMs. However, it does not affect the performance of the DHI strategy for the capacitor voltage ripples suppression effect of the two types of SMs.

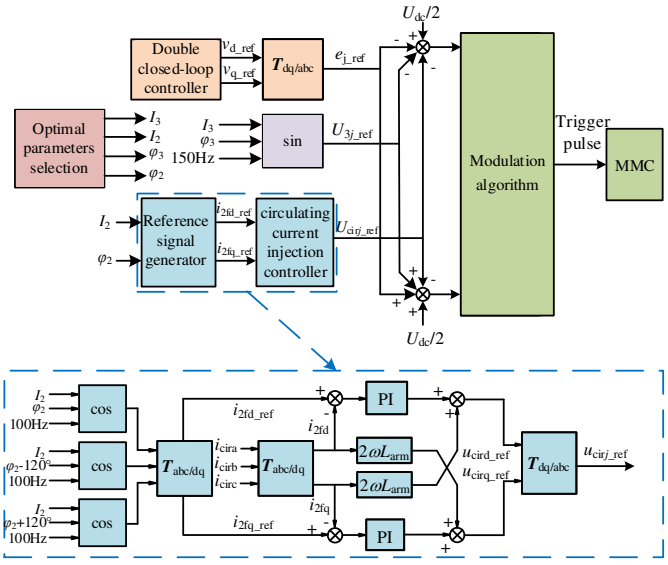

Fig. 4. Control diagram of the DHI.

The dashed block in Fig. 4 shows the reference signal generator and the SHCI controller. i_{cira}, i_{cirb} and i_{circ} are the measured values of the circulating current of phases A, B and C. i_{2fd} and i_{2fq} are the d-axis and q-axis double-frequency circulating currents. i_{2fd_ref} and i_{2fq_ref} are their references. u_{cird_ref} and u_{cirq_ref} are the d-axis and q-axis modulation voltage references. The modulation voltage reference signal U_{cirj_ref} is

generated by the *d-q* inverse transformation of u_{cird_ref} and u_{cirq_ref}.

V. Simulation Results

A. System Parameters

To verify the effectiveness of the proposed DHI strategy, simulations have been conducted in PSCAD. Parameters of the hybrid MMC model are shown in Table I.

TABLE I
PARAMETERS

Items	Values
Grid-side voltage (rms)	380 kV
Valve-side voltage (rms)	245 kV
Modulation index	1
Rated power	800 MW
DC voltage	400 kV
Arm inductor	0.133 H
Transformer leakage inductance	0.1 p.u.
Number of FB-SMs	120
Number of HB-SMs	120
Capacitance of SM	5500 μF
Rated capacitor voltage	2 kV

B. Analysis of Multi-Condition Simulation Results

This subsection will analyze two forms of voltage dips: the voltage of phase *A* drops to 0 (solid SLG fault) and the voltages of phases *A* and *B* drop to 0.5 p.u.

1) *SLG fault in Phase A*

When an SLG fault occurs in phase *A*, the three-phase voltages will be unbalanced. From the analysis in Section II, the positive-sequence voltage modulation index is $m_a^+ = m_b^+ = m_c^+ = 2m/3$, the negative-sequence voltage modulation index is $m_a^- = m_b^- = m_c^- = m/3$, the angles α^+ & α^- of phase *A* are 0° and 120°, the angles β^+ & β^- of phase *B* are -120° and 0° and the angles γ^+ & γ^- of phase *C* are both 120°. The optimal parameters for DHI under this condition are obtained by calculation in Fig.3, where the parameters k_2 and φ_2 of the SHCI are 0.3 and -85.46°, and the parameters k_3 and φ_3 of THVI are -0.3 and 175.23°, and the optimum modulation index m_{opt} is 1.3. The simulation results are shown in Fig. 5.

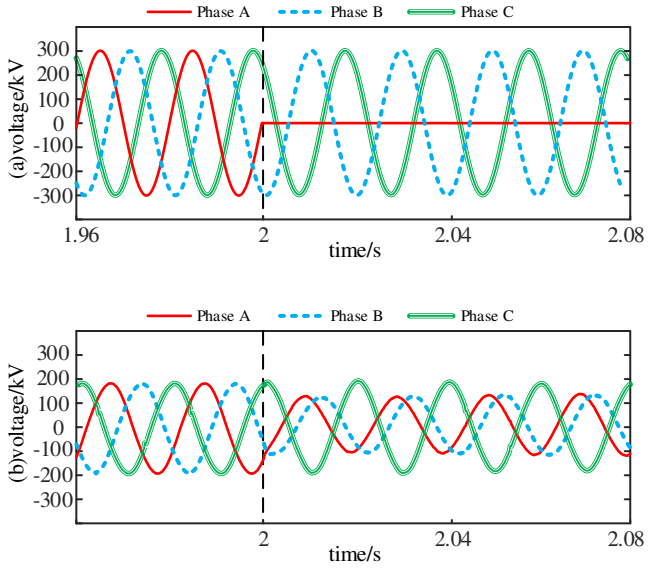

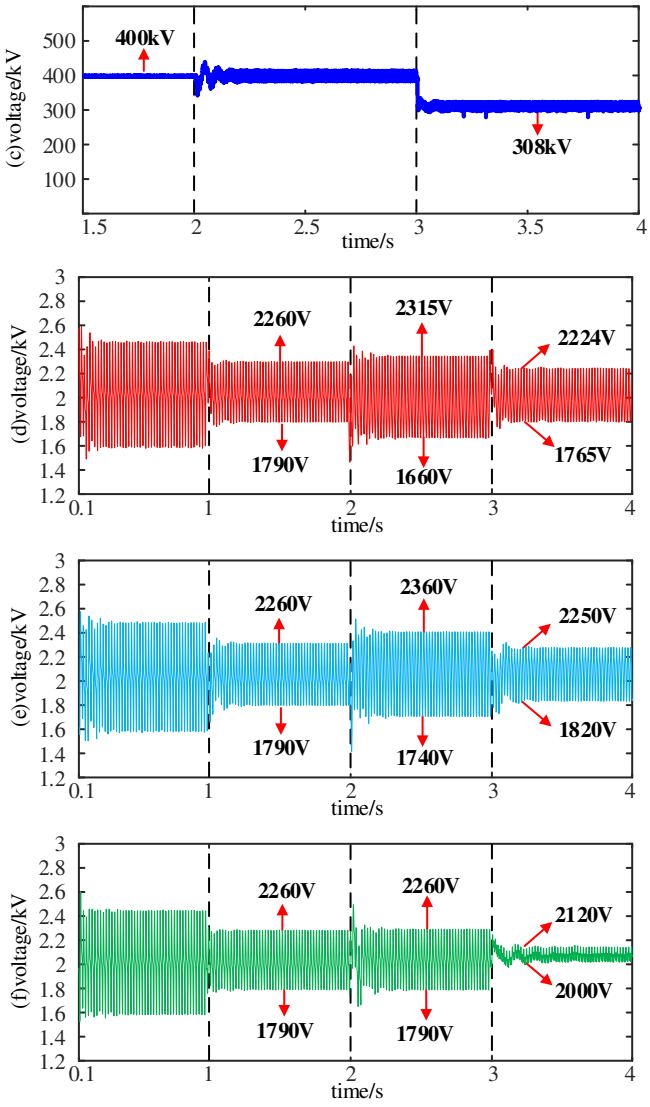

Fig. 5. Simulation results under SLG fault. (a) Grid-side AC voltage, (b) valve-side AC voltage, (c) DC voltage, (d) capacitor voltage of phase *A*, (e) capacitor voltage of phase *B*, (f) capacitor voltage of phase *C*.

Fig. 5(a) shows the three-phase AC voltage on the grid side, and the SLG fault occurs in phase *A* at t = 2 s. Fig. 5(b) shows the three-phase AC voltage on the valve side. The simulation results are consistent with the theoretical analysis in Section II. To avoid the arm overcurrent during the SLG fault, the rated transmission power is reduced by one-third. In Fig. 5(c), the strategy proposed is triggered at t = 3 s, while the DC voltage decreases from 400 kV to 308 kV to achieve the optimal modulation index. Figs. 5(d), (e) and (f) show the capacitor voltage of the three-phase SMs, from which it can be seen that the voltage ripples of thethree-phase increase significantly after the SLG fault. Compared with the period of SLG fault, after applying the proposed strategy, the amplitudes of capacitor voltage ripples of phases *A*, *B* and *C* are reduced from 655 V to 459 V, 620 V to 430 V and 470 V to 120 V, and the reduction rates of phases *A*, *B* and *C* are 29.92%, 30.65% and 74.47%. It indicates that the proposed strategy has an excellent suppression effect on the capacitor voltage ripples of the three-phase SMs under SLG fault.

2) *Voltage Dips on Phases A and B*

The voltages of phases *A* and *B* drop to 0.5 p.u. and the grid voltage is unbalanced. According to analysis, the positive sequence voltage modulation index is $m_a^+=m_b^+=m_c^+=2m/3$, the negative-sequence voltage modulation index is $m_a^-=m_c^-=-m/6$ and $m_b^-=m/6$, the angles α^+ & α^- of phase *A* are 0° and 120°, the angle β^+ & β^- of phase *B* are -120° and 60° and the angle γ^+ & γ^- of phase *C* are 120° and 0°. The optimal parameters for DHI under this condition are obtained by calculation in Fig.3, where the parameters k_2 and φ_2 of the SHCI are -0.3 and 89.29°, and the parameters k_3 and φ_3 of THVI are -0.3 and -180°, and the optimum modulation index m_{opt} is 1.5. The simulation results are shown in Fig. 6.

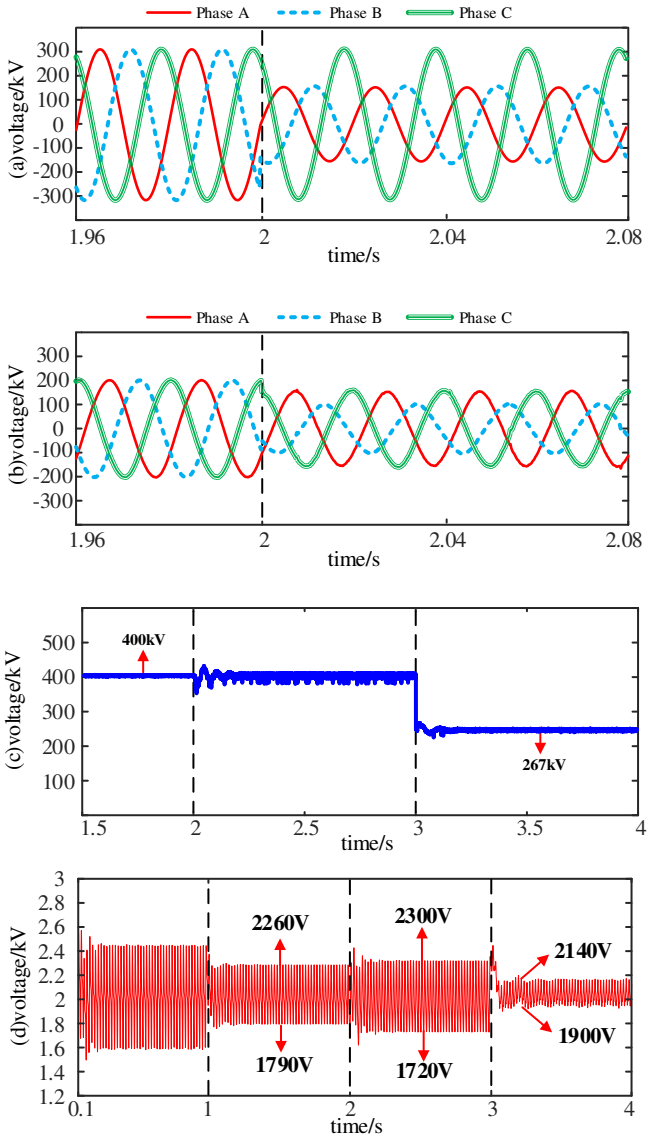

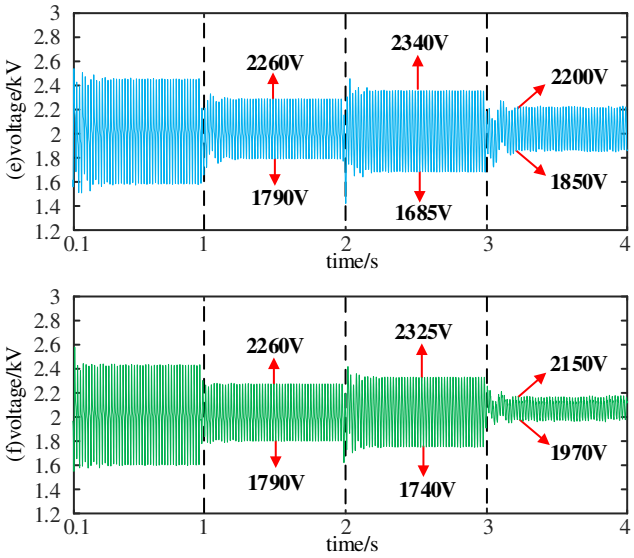

Fig. 6. Simulation results under two-phase voltage dips. (a) Grid-side AC voltage, (b) valve-side AC voltage, (c) DC voltage, (d) capacitor voltage of phase *A*, (e) capacitor voltage of phase *B*, (f) capacitor voltage of phase *C*.

Fig. 6(a) shows the three-phase AC voltage on the grid side, and the two-phase voltage dips occurs in phase *A* and *B* at $t = 2$ s, the three-phase voltages are unbalanced. Fig. 6(b) shows the three-phase AC voltage on the valve side. Similarly, to avoid overcurrent in the arm during the voltage dips, so the rated transmission power is reduced by one-third. In Fig. 6(c), the strategy proposed is activated at $t = 3$ s, while the DC voltage decreases from 400 kV to 267 kV to achieve the optimal modulation index. Figs. 6(d), (e) and (f) show the capacitor voltages of the three-phase SMs, from which it can be seen that the voltage ripples of the three phases increase significantly after the voltage dips. Compared with the period of voltage dips, after applying the proposed strategy, the amplitudes of capacitor voltage ripples of phases *A*, *B* and *C* are reduced from 580 V to 240 V, 655 V to 350 V and 585 V to 180 V, and the reduction rates of phases *A*, *B* and *C* are 58.62%, 46.56% and 69.23%. It indicates that the proposed strategy has good suppression performance on the capacitor voltage ripples of the three-phase SMs under two-phase voltage dips.

3) *Three-Phase Voltage Dips*

When the three-phase voltages drop to 0.8 p.u., the grid voltage will remain balanced. There will be no negative-sequence component on the valve-side of MMC, the three-phase positive sequence voltage modulation index m^+ is $0.8m$, and the rest of the parameters are consistent with the steady-state condition. The optimal parameters for DHI under this condition are obtained by calculation in Fig.3, where the parameters k_2 and φ_2 of the SHCI are -0.4 and 86.42°, and the parameters k_3 and φ_3 of THVI are 0.4 and -8.11°, and the optimum modulation index m_{opt} is 1.5 The simulation results are shown in Fig. 7.

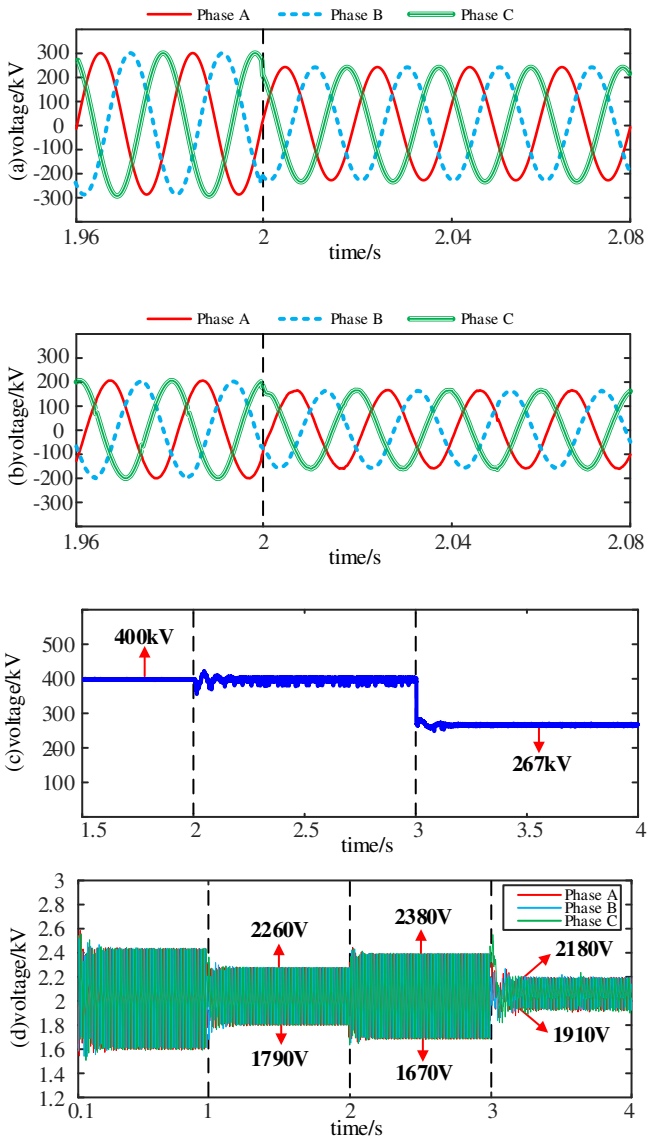

Fig. 7. Simulation results under three-phase voltage sag condition. (a) Grid-side AC voltage, (b) valve-side AC voltage, (c) DC voltage, (d) three-phase capacitor voltage.

Figs. 7(a) and (b) show the three-phase AC voltages on the grid-side and valve-side of the MMC. The three-phase voltage drops to 0.8 p.u. at $t = 2$ s. In Fig. 7(c), the proposed strategy is applied at $t = 3$ s, while the optimal modulation index m_{opt} is achieved by reducing the DC voltage from 400 kV to 267 kV. As can be seen from Fig. 6(d), compared with the period of voltage dips, the amplitude of the SM capacitor voltage ripples drops from 710 V to 270 V after the proposed strategy is applied, which is a 61.97% reduction. It indicates that the proposed strategy is effective under three-phase voltage dips.

VI. Comparison with Other Strategies

The proposed strategy in this paper and the one in [26] are both DHI strategies, and the differences between them are mainly in two aspects. First, the proposed strategy considers the second-order harmonic voltage on the arm inductor, therefore, the arm voltage model is more accurate. Second, the strategy in [26] only considers the steady-state condition, the strategy proposed in this paper is suitable for both the steady-state condition and various unbalanced voltage conditions. To make a comparison between the two methods, simulations have been conducted and are shown in Figs. 8 and 9. The strategy in [26] is defined as the traditional strategy.

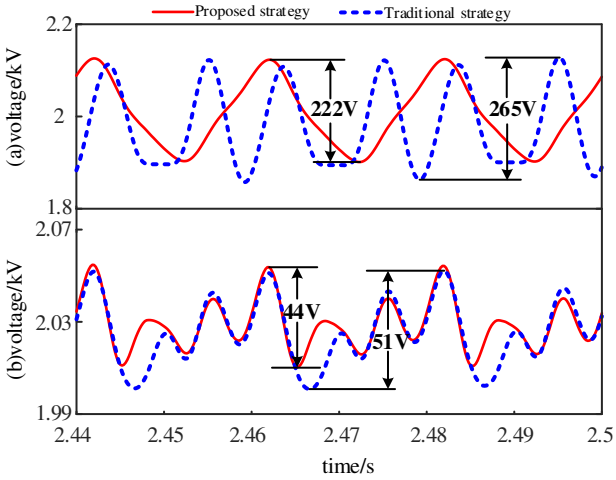

Fig. 8. SM capacitor voltages under steady-state condition. (a) m=0.85, cosφ=1, (b) m=1.2, cosφ=1.

In Fig. 8(a), the optimization of parameter (k_2, k_3, φ_2, φ_3, m_{opt}) with proposed strategy is (0.4, 0.1, 270.44°, 292.21°, 0.85) and that with traditional strategy is (1.426, 0, -90°, 0, 0.85). In Fig. 8(b), the optimization of parameter with proposed strategy is (-0.5, 0.2, 91.67°, 311.69°, 1.2) and that with traditional strategy is (-0.5272, -0.1379, 89.86°, 178.67°, 1.2). According to Fig. 8(a), under stead-state condition, the amplitude of capacitor voltage ripples applying the traditional strategy is 265 V, while the proposed strategy is 222 V, the capacitor voltage ripple is suppressed by 16.23%. It can be seen from Fig. 8(b) that the amplitude of capacitor voltage ripples applying the traditional strategy is 51 V, while the proposed strategy is 44 V, the capacitor voltage ripple is suppressed by 13.73%.

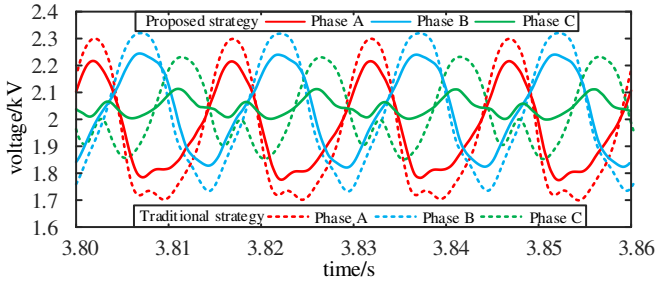

Fig. 9. SM capacitor voltages under an SLG fault(m=1, cosφ=1).

In Fig. 9, the optimization of parameter with the proposed strategy is (0.3, -0.3, -85.46°, 175.23°, 1.3) and that with traditional strategy is (0.7087, 0.4111, -89.47°, 179.24°, 1). According to Fig. 9, after applying the traditional strategy, the voltage ripple reduction rates of phases *A*, *B*, and *C* under SLG fault in phase *A* are 9.23%, 8.46% and 19.15%, while the proposed strategy are 29.92%, 30.65% and 74.47%.

The strategy in [28] is an SHCI strategy for grid-side SLG faults, and the differences between it and the proposed strategy are in three aspects. First, the proposed strategy considers the second-order harmonic voltage on the arm inductor, therefore,

the arm voltage model is more accurate. Second, the proposed strategy is a DHI strategy and the one in [28] is an SHCI strategy. Third, the strategy in [28] only considers the SLG fault condition, other unbalanced voltage conditions are not investigated. To make a comparison between the two methods, simulations have been conducted and are shown in Fig. 10. The strategy in [28] is defined as the SLG strategy.

In Fig. 10, the optimization of parameter with the proposed strategy is (-0.3, 0.3, 103.61°, 29.13°, 1.3) and that with SLG strategy is (0.5, 0, 270.44°, 0, 1.2). According to Fig. 10, after applying the SLG strategy, the voltage ripple reduction rates of phases *A*, *B*, and *C* under an SLG fault in phase *A* are 10.57%, 13.46% and 59.09%, while the proposed strategy are 17.31%, 19.23% and 66.67%. The results show that the proposed strategy is more effective in suppressing the capacitor voltage ripples under SLG faults compared to the SLG strategy.

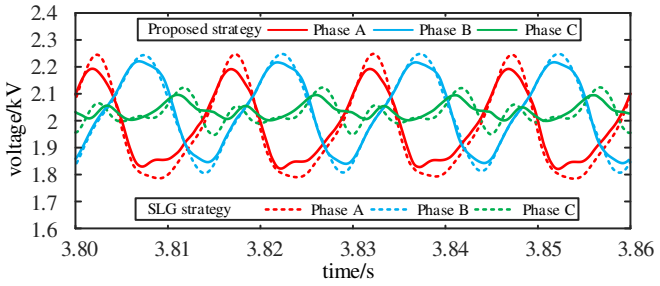

Fig. 10. SM capacitor voltages under an SLG fault(m=1.2, cosφ=1).

Through the above comparisons, it can be seen that the proposed strategy in this paper is more effective in suppressing the capacitor voltage ripples under steady-state condition and SLG faults compared to the traditional strategy and the SLG strategy. Besides, the proposed strategy can be applied to more unbalanced voltage conditions, such as two-phase and three-phase voltage dips conditions, which have not been studied.

VII. Conclusion

To reduce the cost and volume/weight of hybrid MMCs and mitigate SM overvoltage of under unbalanced voltages, this paper proposes a dual harmonic injection strategy. By injecting the second-order harmonic current and the third-order harmonic voltage, the waveforms of the arm current and AC voltage are reshaped. The proposed strategy can effectively reduce the fundamental-frequency and double-frequency components of the arm power by optimizing the modulation index and the injection parameters, and therefore suppress SM capacitor voltage ripples.

Simulation results show that the unbalanced grid voltage will aggravate the capacitor voltage fluctuations of the SMs. However, the proposed strategy can greatly reduce the capacitor voltage ripples under typical unbalanced grid voltage conditions. Compared with the classical circulating current suppression strategy, it can further suppress more than 50% of capacitor voltage fluctuations, which can reduce the demand for SM capacitance and can also effectively avoid SM overvoltage under unbalanced voltage conditions.

References

[1] S. Debnath, J. Qin, B. Bahrani, M. Saeedifard and P. Barbosa, "Operation, Control, and Applications of the Modular Multilevel Converter: A Review," *IEEE Trans. Power Electron.,* vol. 30, no. 1, pp. 37-53, Jan. 2015.

[2] J. A. Ferreira, "The Multilevel Modular DC Converter," *IEEE Trans. Power Electron.*, vol. 28, no. 10, pp. 4460-4465, Oct. 2013.

[3] D. C. Ludois and G. Venkataramanan, "Simplified Terminal Behavioral Model for a Modular Multilevel Converter," *IEEE Trans. Power Electron.*, vol. 29, no. 4, pp. 1622-1631, April 2014.

[4] Y. Li, E. A. Jones and F. Wang, "The impact of voltage-balancing control on switching frequency of the modular multilevel converter," *IEEE Trans. Power Electron.*, vol. 31, no. 4, pp. 2829-2839, April 2016.

[5] M. C. Merlin and T. Green, "Cell capacitor sizing in multilevel converters: cases of the modular multilevel converter and alternate arm converter," *IET Power Electron.*, vol.8, no.3, pp. 350-360, Jan.2015.

[6] M. Guan and Z. Xu, "Modeling and Control of a Modular Multilevel Converter-Based HVDC System Under Unbalanced Grid Conditions," *IEEE Trans. Power Electron.*, vol. 27, no. 12, pp. 4858-4867, Dec. 2012.

[7] Q. Tu and Z. Xu, "Impact of Sampling Frequency on Harmonic Distortion for Modular Multilevel Converter," *IEEE Trans. Power Del.*, vol. 26, no. 1, pp. 298-306, Jan. 2011.

[8] M. Vasiladiotis, N. Cherix and A. Rufer, "Accurate Capacitor Voltage Ripple Estimation and Current Control Considerations for Grid-Connected Modular Multilevel Converters," *IEEE Trans. Power Electron.,* vol. 29, no. 9, pp. 4568-4579, Sept. 2014.

[9] B. Li, Z. Xu, S. Shi, D. Xu and W. Wang, "Comparative Study of the Active and Passive Circulating Current Suppression Methods for Modular Multilevel Converters," *IEEE Trans. Power Electron.*, vol. 33, no. 3, pp. 1878-1883, March 2018.

[10] X. Yu, Y. Wei, Q. Jiang, X. Xie, Y. Liu, and K. Wang, "A novel hybrid arm bipolar MMC topology with dc fault ride-through capability," *IEEE Trans. Power Del.*, vol. 32, no. 3, pp. 1404–1413, May 2017.

[11] J. Hu, K. Xu, L. Lin, and R. Zeng, "Analysis and enhanced control of hybrid-MMC-based HVDC systems during asymmetrical DC voltage faults," *IEEE Trans. Power Del.*, vol. 32, no. 3, pp. 1394–1403, Jun. 2017.

[12] R. Zeng, L. Xu, L. Yao, and B. W. Williams, "Design and operation of a hybrid modular multilevel converter," *IEEE Trans. Power Electron.*, vol. 30, no. 3, pp. 1137–1146, Mar. 2015.

[13] R. Zeng, L. Xu, L. Yao, and D. John Morrow, "Precharging and DC fault ride-through of hybrid MMC-based HVDC systems," *IEEE Trans. Power Del.*, vol. 30, no. 3, pp. 1298–1306, Jun. 2015.

[14] P. D. Judge, G. Chaffey, M. M. C. Merlin, et al., "Dimensioning and Modulation Index Selection for the Hybrid Modular Multilevel Converter," *IEEE Trans. Power Electron.*, vol. 33, no. 5, pp. 3837-3851, May. 2018.

[15] W. Lin, D. Jovcic, S. Nguefeu and H. Saad, "Full-Bridge MMC Converter Optimal Design to HVDC Operational Requirements," *IEEE Trans. Power Del.*, vol. 31, no. 3, pp. 1342-1350, Jun. 2016.

[16] G. Li, *et al.*, "Feasibility and Reliability Analysis of LCC DC Grids and LCC/VSC Hybrid DC Grids," *IEEE Access*, vol. 7, pp. 22445-22456, 2019.

[17] B. Li, Y. Zhang, G. Wang, W. Sun, D. Xu and W. Wang, "A Modified Modular Multilevel Converter With Reduced Capacitor Voltage Fluctuation," *IEEE Trans Ind. Electron.*, vol. 62, no. 10, pp. 6108-6119, Oct. 2015.

[18] Q. Yang, R. B. Gonzatti, H. Pourgharibshahi and F. Peng, "Capacitor Voltage Ripple Suppression of the Switched Capacitor Modular Multilevel Converter," *2021 IEEE Energy Conversion Congress and Exposition (ECCE)*, 2021, pp. 1932-1938.

[19] Q. Tu, Z. Xu and L. Xu, "Reduced Switching-Frequency Modulation and Circulating Current Suppression for Modular Multilevel Converters," *IEEE Trans. Power Del.*, vol. 26, no. 3, pp. 2009-2017, July 2011.

[20] R. Picas, J. Pou, S. Ceballos, V. G. Agelidis and M. Saeedifard, "Minimization of the capacitor voltage fluctuations of a modular multilevel converter by circulating current control," in *Proc. 38th Annu. Conf. IEEE Ind. Electron. Soc*., 2012, pp. 4985–4991.

[21] J. Wang, X. Han, H. Ma and Z. Bai, "Analysis and Injection Control of Circulating Current for Modular Multilevel Converters," *IEEE Trans. Ind. Electron.*, vol. 66, no. 3, pp. 2280-2290, March 2019.

[22] C. Zhao *et al*., "Energy Storage Requirement Optimization of Hybrid Modular Multilevel Converter With Circulating Current Injection," *IEEE Trans. Ind. Electron.*, vol. 66, no. 9, pp. 6637-6648, Sept. 2019.

[23] C. Zhao *et al*., "Energy Storage Requirements Optimization of Full-Bridge MMC With Third-Order Harmonic Voltage Injection," *IEEE Trans. Power Electron.*, vol. 34, no. 12, pp. 11661-11678, Dec. 2019.
[24] R. Li, J. Fletcher, and B. Williams. "Influence of third harmonic injection on modular multilevel converter -based high-voltage direct current transmission systems," *IET Gener.*, *Transmiss. Distrib.*, vol. 10, no. 11, pp. 2764-2770, Dec. 2016.
[25] J. Pou, S. Ceballos, G. Konstantinou, V. G. Agelidis, R. Picas and J. Zaragoza, "Circulating Current Injection Methods Based on Instantaneous Information for the Modular Multilevel Converter," *IEEE Trans. Ind. Electron.*, vol. 62, no. 2, pp. 777-788, Feb. 2015.
[26] J. Xu *et al*., "Dual Harmonic Injection for Reducing the Submodule Capacitor Voltage Ripples of Hybrid MMC," *IEEE Trans. Emerg. Sel. Topics Power Electron.*, vol. 9, no. 3, pp. 3622-3633, June 2021.
[27] M. Vasiladiotis, N. Cherix and A. Rufer, "Impact of Grid Asymmetries on the Operation and Capacitive Energy Storage Design of Modular Multilevel Converters," *IEEE Trans. Ind. Electron.*, vol. 62, no. 11, pp. 6697-6707, Nov. 2015.
[28] J. Xu, W. Deng, G. Li, C. Zhao and C. Liu, "Optimal Second-Harmonic Current Injection for Capacitor Voltage Fluctuation Reduction in Hybrid MMCs Under Grid-side SLG Faults," *IEEE Trans. Power Del.*, (Early Access)
[29] C. Zhao, F. Gao, Z. Li, P. Wang and Y. Li, "Modulation Index Design of Full-Bridge MMC for Capacitor Voltage Ripples Reduction Under Single-Line-to-Ground Faults Conditions," *IEEE Trans. Power Del.*, vol. 36, no. 3, pp. 1775-1784, June 2021
[30] L. Lin, Y. Lin, C. Xu and Y. Chen, "Comprehensive Analysis of Capacitor Voltage Fluctuation and Capacitance Design for Submodules in Hybrid Modular Multilevel Converter With Boosted Modulation Index," *IEEE Journal of IEEE Trans. Emerg. Sel. Topics Power Electron.*, vol. 7, no. 4, pp. 2369-2383, Dec. 2019.

Jianzhong Xu (M'14-SM'19) was born in Shanxi, China. He received the B.S. and Ph.D. degrees from North China Electric Power University (NCEPU) in 2009 and 2014 respectively. Currently, he is an Associate Professor and Ph.D. Supervisor of the State Key Laboratory of Alternate Electrical Power System with Renewable Energy Sources, North China Electric Power University, China, where he obtained his Ph.D. degree in 2014. From 2012 to 2013 and 2016 to 2017, he was a visiting Ph.D. student and Post-Doctoral Fellow at the University of Manitoba, Canada. He is an Associate Editor of the CSEE Journal of Power and Energy Systems. He is now working on the Electromagnetic Transient (EMT) equivalent modelling, fault analysis and protection of HVDC Grids.

Junxin Wang was born in Henan, China. he received the B.S. degree in power system and its automation from Dalian Maritime University (DMU) in 2020, and he is currently working toward his master degree in North China Electric Power University (NCEPU). His research interests include HVdc grid operation and protection.

Yukun Yang was born in Henan, China. he received the B.S. degree in power system and its automation from Tiangong University (TGU) in 2021, and he is currently working toward his master degree in North China Electric Power University (NCEPU). His research interests include HVdc grid operation and protection.

Jin'an Wang was born in Zhejiang, China. She received the B.S. degree in Electrical Engineering and Its Automation from North China Electric Power University (NCEPU) in 2020, where she is currently working toward her master degree. Her research interests include HVdc grid operation and energy storage technology.

Gen Li (M'18) received the B.Eng. degree in Electrical Engineering and its Automation from Northeast Electric Power University, Jilin, China, in 2011, the M.Sc. degree in Power Engineering from Nanyang Technological University, Singapore, in 2013 and the Ph.D. degree in Electrical Engineering from Cardiff University, Cardiff, U.K., in 2018.

From 2013 to 2016, he was a Marie Curie Early Stage Research Fellow funded by the European Union's MEDOW project. He has been a Visiting Researcher at China Electric Power Research Institute and Global Energy Interconnection Research Institute, Beijing, China, at Elia, Brussels, Belgium and at Toshiba International (Europe), London, U.K. He has been a Research Associate at the School of Engineering, Cardiff University since 2017. His research interests include control and protection of HVDC and MVDC technologies, power electronics, reliability modelling and evaluation of power electronics systems.

Dr. Li is a Chartered Engineer in the U.K. He is an Associate Editor of the CSEE Journal of Power and Energy Systems. He is an Editorial Board Member of CIGRE ELECTRA. He is an IET Professional Registration Advisor. His Ph.D. thesis received the First CIGRE Thesis Award in 2018. He is the Vice-Chair of IEEE PES Young Professionals and the Technical Panel Sectary of CIGRE UK B5 Protection and Automation.